Neurobiol Dis. Author manuscript; available in PMC 2010 June 15.

Published in final edited form as:
Neurobiol Dis. 2006 May ; 22(2): 302–311. doi:10.1016/j.nbd.2005.11.014.

Gene expression profiling in frataxin deficient mice: Microarray evidence for significant expression changes without detectable neurodegeneration

Giovanni Coppola[a,1], **Sang-Hyun Choi**[a,b,1], **Manuela M. Santos**[c], **Carlos J. Miranda**[c], **Dmitri Tentler**[a], **Eric M. Wexler**[a], **Massimo Pandolfo**[d], and **Daniel H. Geschwind**[a,*]

[a] Program in Neurogenetics, Department of Neurology, David Geffen School of Medicine-UCLA, 710 Westwood Plaza, Los Angeles, CA 90095, USA

[b] Department of Pharmacology, Korea University College of Medicine, Seoul 136-705, South Korea

[c] Centre de Recherche, CHUM-Hôpital Notre-Dame, Montréal, Québec, Canada H2L 4M1

[d] Service de Neurologie, Université Libre de Bruxelles-Hôpital Erasme, Brussels, Belgium

Abstract

Friedreich's ataxia (FRDA) is caused by reduction of frataxin levels to 5–35%. To better understand the biochemical sequelae of frataxin reduction, in absence of the confounding effects of neurodegeneration, we studied the gene expression profile of a mouse model expressing 25–36% of the normal frataxin levels, and not showing a detectable phenotype or neurodegenerative features. Despite having no overt phenotype, a clear microarray gene expression phenotype was observed. This phenotype followed the known regional susceptibility in this disease, most changes occurring in the spinal cord. Additionally, gene ontology analysis identified a clear mitochondrial component, consistent with previous findings. We were able to confirm a subset of changes in fibroblast cell lines from patients. The identification of a core set of genes changing early in the FRDA pathogenesis can be a useful tool in both clarifying the disease process and in evaluating new therapeutic strategies.

Keywords

Friedreich's ataxia; Microarray; Mouse model; Frataxin; Neurodegeneration; Knockin/knockout

Introduction

Friedreich ataxia (FRDA), the most prevalent inherited ataxia, is most frequently caused by a GAA triplet repeat expansion within the first intron of the gene encoding for frataxin, a nuclear encoded mitochondrial protein (Campuzano et al., 1996). The mutation affects frataxin transcription, leading to severe reduction of protein levels in homozygous patients

*Corresponding author. Fax: +1 310 267 2401. dhg@ucla.edu (D.H. Geschwind).
[1]These authors equally contributed to this work.

(Bidichandani et al., 1998). The normal function of frataxin, and how its deficiency ultimately leads to neuronal dysfunction and death, is not well understood. Deficiency of the yeast frataxin homolog protein Yfh1p causes a strong reduction in the assembly of mitochondrial proteins containing iron–sulfur clusters (ISC) (Muhlenhoff et al., 2002), and frataxin is required for ISC assembly in yeast mitochondria (Gerber et al., 2003; Lutz et al., 2001). These data support a specific role for frataxin in the biosynthesis of cellular ISC proteins, which may be in turn related to oxidative stress sensitivity and iron homeostasis alterations (Puccio and Koenig, 2002).

FRDA has been a challenging disease to model in mice. Homozygous deletion of frataxin in the mouse causes embryonic lethality a few days after implantation, demonstrating a pivotal role for frataxin during early development (Cossee et al., 2000). Heterozygous knockout mice show reduced (50%) frataxin levels, no obvious phenotype, and sporadic heart iron deposits after dietary iron load (Santos et al., 2003). Through a conditional gene-targeting approach, neuronal, cardiac (Puccio et al., 2001), and pancreatic (Ristow et al., 2003) frataxin knockout mice have been generated. These models show cardiac hypertrophy, large sensory neuron dysfunction, deficient ISC protein activities (Puccio et al., 2001), and diabetes due to reactive oxygen species increase, growth arrest, and apoptosis in pancreatic beta cells (Ristow et al., 2003).

However, in FRDA patients (Pianese et al., 2004) and in lymphoblastoid cell lines derived from FRDA patients (Campuzano et al., 1997) a residual frataxin activity (5–35% of normal levels) is present. Thus, animal models with FRDA reduction, rather than its complete absence, would be valuable to further explore the effects of moderate frataxin deficiency on cellular and organismal functioning. One such model has involved the generation of a mouse expressing frataxin only from a human transgene containing a small repeat expansion (Miranda et al., 2002). The presence of a homozygous $(GAA)_{230}$ repeat expansion in *frda* mouse gene led to a reduction of frataxin levels to about 75% of the wild type (WT). After crossing this knockin mouse with a frataxin knockout, the resulting knockin/knockout offspring (KIKO) expressed 25–36% of the WT levels. These mice – when examined at 12 months of age – showed no obvious phenotype, no iron deposits, and no differences with controls after dietary and parenteral iron load (Miranda et al., 2002). This model therefore provides a significant advantage for gene expression studies aimed at understanding the consequences of frataxin deficiency, since it is not confounded by factors that often accompany but may not initiate neurodegeneration, such as cell loss or inflammation (Geschwind, 2000).

FRDA presents a striking regional distribution of neuropathological abnormalities, with constant involvement of cervical spinal cord, neuronal loss in brainstem nuclei, and fairly common loss of Purkinje cells in the cerebellar cortex (Lamarche et al., 1984). To address the FRDA regionality, we studied several brain regions from KIKO mice using DNA microarrays. We hypothesized that, at a time prior to any evidence of neurodegeneration, this would allow us to assess early cellular changes in tissues that were frataxin deficient, in the absence of detectable cell loss. Similar approaches have been used to assess biochemical changes prior to the onset of overt disease in other models of neurodegenerative conditions, such as spinocerebellar ataxia (SCA) 1 (Serra et al., 2004), ataxia with vitamin E deficiency

(AVED) (Gohil et al., 2003), amyotrophic lateral sclerosis (Yoshihara et al., 2002), Huntington's disease (Sipione et al., 2002), and in heterozygous carriers of ataxia telangiectasia (Watts et al., 2002). This approach has allowed us to gain insight into early molecular dysfunction caused by reduced frataxin levels and complements other recent studies in this area by highlighting key pathways for therapeutic intervention.

Materials and methods

Samples

Frataxin heterozygous knockout mice ($frda^{+/-}$) were crossed with $frda^{+/230GAA}$ mice, to generate frataxin knockout/knockin mice ($frda^{-/230GAA}$) and the offspring was genotyped as described (Miranda et al., 2002). In this study, four 6-month-old KIKO mice were compared to age and gender matched WT littermates. Total RNA from three brain regions, cervical spinal cord (SC), cerebellum (CB), and brainstem (BS), was extracted by acid phenol extraction (Trizol, GIBCO/BRL) as recommended by the manufacturer. The purity and quality of the extracted RNA were assayed by measuring the optical density at 260 and 280 nm (NanoDrop ND-100 Spectrophotometer, NanoDrop Technologies) and by gel electrophoresis on RNA assay chips (Agilent 2100 Bioanalyzer, Agilent Technologies). Four WT (two males and two females) and four KIKO (two males and two females) mice were compared. RNAs from WT samples of the same gender were pooled, and co-hybridized with KIKO samples (Fig. 1).

Probe synthesis and hybridization

Labeled cDNA synthesis, hybridization, and signal detection were performed using the tyramide signal amplification (TSA, PerkinElmer) kit, according to the manufacturer's protocols with minor modifications (Karsten et al., 2002). Briefly, two total RNA samples (1.5 μg) were reverse transcribed to fluorescein- and biotin-labeled cDNA, and hybridized on mouse 9K cDNA arrays (UCLA Microarray Core Facility, http://www.genetics.u-cla.edu/microarray), including 9,150 genes and expressed sequence tags. This cDNA array based on the Incyte Unigem 1 mouse clone set was chosen because it had previously shown highly reproducible hybridizations (Karsten and Geschwind, 2002; Karsten et al., 2002). Probe signals were generated using Cy3 and Cy5 reporters, and the hybridization was duplicated with dye swapping, in order to eliminate the influence of dye bias effects (Liang et al., 2003; Yang et al., 2002). Eight hybridizations using 4 independent pairs were performed for each of the three brain regions, for a total of 24 microarray hybridizations. Two additional microarrays were used for homotypic control/control hybridizations.

Scanning and data analysis

Slides were scanned by the GMS 418 Array Scanner (Genetic Microsystems), and the resulting images were analyzed by ImaGene 4.2 (Biodiscovery) using auto segmentation measurements set 3 pixel buffer and width for background. Signals from the poor quality spots flagged by ImaGene software were ignored. The ImaGene-generated data were loaded onto Gene-Spring 6.0 (Silicon Genetics), the local background was subtracted, and only the signal intensities greater than the background were subjected to lowess normalization, to obtain intensity-dependent normalized ratios of KIKO to WT. After averaging the dye-

swapped ratio pairs, every probe had at maximum 4 ratios for each of the three brain regions. EntrezGene (http://www.ncbi.nlm.nih.gov/entrez/), Ensembl (http://www.ensembl.org), and GeneOntology (http://www.geneontology.org) were used to obtain nomenclature, sequence, and gene ontology (GO) information.

Statistical analysis

After ruling out the signal outliers, genes with at least 8 ratio measurements were analyzed by the one-sample Student's *t* test, to select those differentially expressed across all the examined regions. In addition, one-way ANOVA with post hoc Tukey test was used to select those with specific regional changes. By means of EASE software (Hosack et al., 2003) differentially expressed genes with GO data available were searched for over-represented classes. EASE calculates the over-representation (within the subset of differentially expressed genes) of each GO functional cluster, with respect to the total number of genes assayed and annotated within each functional cluster.

Human cell lines

Primary fibroblast cell lines from 3 patients and 3 controls were obtained from Coriell Cell Repositories (Camden, NJ) and cultured in F12 Dulbecco's modified essential medium with HEPES and glutamine (F12-DMEM, Invitrogen), with 10% calf serum and 1% penicillin–streptomycin. All cell lines were cultured at 37°C, in a humidified atmosphere of 5% CO_2, 95% air.

Real-time quantitative PCR

Selected differentially expressed genes were assayed using real-time quantitative PCR (qRT-PCR) using SYBR green I as fluorescent dye. Total RNA (2 μg) from different animals (distinct from those studied in the microarray analysis) was treated with DNAse I (Promega) and converted into cDNA by SuperScript II kit (Invitrogen). The reactions were performed with 2× SYBR-green PCR Master Mix (BioRad), in a 25 μl volume. Assays were performed in triplicate, and analyzed using an ABI 7700 instrument (Applied Biosystems). The fold change was calculated using both standard curve analysis and the Pfaffl method (Pfaffl et al., 2002), using *Hprt* as reference gene. For each gene, data from at least 3 KIKO/WT pairs were averaged.

Results

Genes differentially expressed across all the regions

We first identified genes that were differentially expressed across all the examined brain regions. Student's *t* test analysis identified 185 sequences across 12 independent experiments that were significantly differentially expressed between mutant and WT animals. Among these genes, 116 were upregulated and 69 downregulated (Fig. 2). A list of selected differentially expressed sequences according to their proposed biological function is reported in Table 1. The observed changes were small, but statistically significant, with most genes with a fold change between 1.2 (0.2) and 1.5 (0.5), consistent with the little or absent phenotype.

Genes showing region-specific changes

Since FRDA involves degeneration of specific brain regions, rather than global neurodegeneration, it was also interesting to assess regional distinctions between mutant and WT mice. So, we next determined whether any genes were differentially expressed in some brain regions and not in others, identifying potential pathways that could underlie selective compensation or vulnerability. After ANOVA analysis, an additional 105 genes demonstrated a significant regional pattern of differential expression. Strikingly, the cervical spinal cord, which is the region most affected in the human disease, showed the most changes in gene expression ($n = 61$), followed by brainstem ($n = 27$), and cerebellum ($n = 17$). Moreover, these SC changes were biased to involve more downregulation than upregulation (Fig. 2, Table 1).

Functional categorization of gene expression changes

EASE analysis was used to help annotate genes relative to relevant functional categories. The subset of overall differentially expressed genes (including the genes showing regional changes) was classified according to GO biological process, cellular component, and molecular function (Table 2). Interestingly, the mitochondrial cellular component (along with ribonucleoprotein complex) showed a significant over-representation in this subset of genes, consistent with the mitochondrial localization of the frataxin protein across species, and the demonstrated role of mitochondrial dysfunction in the disease. It is also notable that genes associated with the RNA function and translational regulation were identified in all three gene ontology classifications. The significant over-representation of ribonucleoprotein complex (within cellular components), of RNA binding (within molecular function), and of ribosome biogenesis (within biological function) supports a role for dysfunction in RNA metabolism and protein translation in addition to the basic mitochondrial respiratory involvement in FRDA.

Quantitative RT-PCR confirmation of differential expression

Confirmation on KIKO samples—The expression of 25 genes, chosen to represent a cross section of genes expressed at different levels and regions, was tested on RNA extracted from an independent set of mutant and WT animals, by means of qRT-PCR, so as to provide an independent confirmation of the microarray results (Fig. 3). qRT-PCR data confirmed the microarray data for 18/25 (72%) of the genes.

Confirmation on FRDA fibroblast cell lines—We next tested the expression levels of the human homologs of 11 genes on RNA extracted from three fibroblast cell lines from FRDA patients. 7/11 genes (64%) showed the same changes in human FRDA fibroblasts (Fig. 3). Since fibroblasts are not neural tissue, such a level of confirmation was close to what might be expected a priori, based on experience from our group and others, when confirming changes in different cell types and across different methods (array vs. qRT-PCR).

Discussion

The goal of this microarray study was to identify a biochemical phenotype secondary to a significant reduction in frataxin levels in clinically relevant brain regions, prior to the onset

of any neurodegeneration or clinical phenotype. This avoids confounding factors, as cell loss or reactive changes occurring during overt neurodegeneration. Over 200 differentially expressed genes involved in several pathways were identified. Quantitative RT-PCR was used in independent KIKO mouse samples and in fibroblasts from FRDA patients and confirmed a significant proportion of these changes. A subset of genes showed region-specific changes, mostly involving the cervical spinal cord, which is a region heavily involved in the human disease. Consistent with the subtle biochemical phenotype expected, the magnitude of the changes observed was small, and in many cases likely providing a compensatory mechanism to counteract cellular stress induced by reduced frataxin.

Current pathogenetic theories propose a role of frataxin in ISC assembly (Acquaviva et al., 2005; Muhlenhoff et al., 2002; Stehling et al., 2004), in the activation of stress pathway (Pianese et al., 2002), and in iron metabolism (Cavadini et al., 2002). Microarray studies of Δ*yfh1* yeast strains (knockout for the yeast frataxin homolog) showed increased expression of genes involved in iron level regulation (Foury and Talibi, 2001). In the first study involving human cells, Tan et al. reported altered expression of several classes of genes, including amino acid metabolism, apoptosis and signal transduction; these authors focused on the involvement of the sulfur amino acid pathway (which is connected to the ISC biosynthetic pathway) and confirmed this finding through functional experiments (Tan et al., 2003). In two recent studies, cardiac and liver tissues from a conditional frataxin knock-out were studied with microarrays, and showed expression changes in genes involved in amino acid (Seznec et al., 2005) and heme metabolism (Schoenfeld et al., 2005). In the present study, GO analysis and literature review showed that the genes identified are involved in nucleic acid and protein metabolism, signal transduction, stress response, and nucleic acid binding. The over-representation of mitochondria-related transcripts within the subset of the differentially expressed genes supports an involvement of mitochondrial pathways secondary to the deficiency of frataxin, a nuclear-encoded mitochondrial protein. Thus, our study adds further evidence supporting the mitochondrial and amino acid metabolism involvement, the activation of stress pathways, and little involvement of iron metabolism-related genes in the early steps of FRDA pathogenesis.

OX-REDOX chemistry and disease pathophysiology

Oxidative stress plays an important role in the pathogenesis of FRDA (Puccio and Koenig, 2002), and this may be linked to the ISC biosynthesis defect. Antioxidant defenses have been reported reduced in FRDA cells (Chantrel-Groussard et al., 2001; Jiralerspong et al., 2001), and increased in transgenic cells overexpressing frataxin (Shoichet et al., 2002). Glutathione reductase catalyzes the NADPH-dependent reduction of oxidized glutathione (GSSG) to glutathione (GSH), and is essential in maintaining adequate levels of reduced GSH. Levels of mRNA coding for glutathione reductase 1 are reduced in the cervical spinal cord of frataxin deficient mice, and in fibroblasts from patients. This observation is intriguing, since a lower activity of this enzyme has been reported in the blood of FRDA patients (Helveston et al., 1996) and higher levels of GSSG have been found in frataxin-deficient cells (Tan et al., 2003). The gene *NHL repeat containing 2* has a thioredoxin domain and its transcript is downregulated across all the CNS regions and in FRDA fibroblasts. Thioredoxins play a key role in maintaining proteins in their reduced state, and

in defense against oxidative stress (Arner and Holmgren, 2000). Taken together, our data support the role of an early deficiency in the oxidative stress-related pathways in this animal model, and offer a contribution to the general debate about the role of oxidative stress in neurodegeneration (Andersen, 2004), especially after two recent studies respectively supporting (Sturm et al., 2005) and suggesting a revision (Seznec et al., 2005) of the concept of FRDA as a paradigm for neurodegenerative diseases due to oxidative stress.

The involvement of the stress-pathway response

The mitogen-activated protein kinase (MAPK) signaling cascade is implicated in several cellular processes, including regulation of gene expression in response to environmental stress (Chang and Karin, 2001). A hyperactive stress pathway, involving the mitogen activated protein kinase kinase 4 (*MAP2K4*) and the c-JUN N-terminal kinase was reported in FRDA fibroblasts and in a FRDA foetus, suggesting an early role in the disease pathogenesis (Pianese et al., 2002). *Map4k5*, coding for a member of the MAPK family, is upregulated in frataxin deficient mice. AVED – a human neurodegenerative disorder caused by mutations in the TTPA gene, coding for the α-tocopherol transfer protein – is often clinically indistinguishable from FRDA (Ben Hamida et al., 1993), suggesting some common pathogenetic pathways. Thus, it is striking that the gene expression profile identified here shares some analogies with that of vitamin E deficiency mice. *Map2k3*, a member of the MAPK cascade, is upregulated in the liver of an AVED mouse model (Gohil et al., 2003), and members of the same family have been identified as vitamin E sensitive transcripts (Roy et al., 2002). *RAR-related orphan receptor alpha* (downregulated in brains of KIKO mice and in FRDA fibroblasts) is involved in the lipid metabolism and in protection against age-related degenerative processes (Boukhtouche et al., 2004), and is strongly downregulated in the cortex of $Ttpa^{-/-}$ mice. Of note, the spontaneous *staggerer* mouse is caused by a mutation in this gene, and is associated with ataxia and cerebellar degeneration (Hamilton et al., 1996).

RNA and protein metabolism

The role of RNA and protein metabolism evident in the GO analysis from KIKO mice is supported by other reports in literature. In addition to cysteinyl-tRNA synthetase (upregulated in this study), 3 other tRNA-synthetases (Gln-, Asn-, and Ala-tRNA synthetase) have been reported as upregulated in hearts of *frda* mutants (Seznec et al., 2005), and another (seryl-tRNA synthetase) was previously reported as downregulated in FRDA lymphoblasts (Tan et al., 2003), suggesting an involvement of intracellular amino acid metabolism in the pathogenesis of the disease.

Importance of a ‘microarray phenotype’ in absence of overt neurodegeneration

The presence of a gene expression phenotype raises questions about the absence of a clinical phenotype in this model. The transcriptional profile in KIKO mice may be involved in a compensatory response aimed at maintaining cellular function and integrity, or constitute an early step in disease pathogenesis. In the first case, the compensatory changes would underlie the absent phenotype; in the second, the lifespan of frataxin deficient mice may be too short to detect a clinical phenotype. Therefore, the possibility of a very late-onset disease in this model (or an undetectable underlying pathologic process) should be considered. The

conditional FRDA mouse model shows signs of neurological impairment about 6 months after the knocking-down of frataxin (Simon et al., 2004), and the knockout mouse for α-TTP (α-TTP$^{-/-}$) – a model of a late-onset, slowly progressive neuronal degeneration due to chronic oxidative stress – did not present clinical or pathological phenotype until after 1 year of age (Yokota et al., 2001). But, similar to our observations here, a gene expression phenotype could be detected in a similar model at 12–16 weeks of age (Gohil et al., 2003). Thus, the presence of a detectable phenotype is related to many factors, including age, genetic background, and type of phenotypic analysis. Although fibroblasts are not known to be involved in human disease, they provide an accessible source for comparing in human tissue changes found in mouse. Thus, we do not expect all the changes in brain to be measured in fibroblasts, but we were able to confirm a subset of the genes changing in KIKO mice in FRDA fibroblasts. This provides some additional support for the use of mouse models in this disorder, and additional candidate genes for further investigation through functional studies. In addition, the definition of a core of genes changing due to frataxin deficiency can be useful in the evaluation of small molecules with possible therapeutic value: looking for candidate drugs able to revert a gene expression phenotype based on 10–15 genes may be more sensitive than relying entirely on frataxin levels.

Some methodological issues should be addressed. Even after a conservative statistical approach, some of the detected changes in a microarray study can always be due to biological variability. However, in this case, we reduced this effect by performing many replicates (8 per brain region), pooling the samples, and confirming the differentially expressed genes with qRT-PCR on animals distinct from those tested in the microarray study. A concordance of 72% between qRT-PCR and microarray data is well within typical levels of confirmation, especially using independent samples. In addition, nearly 10% of the observed changes were confirmed in this manner by qRT-PCR, a large cross section of the data. It should be emphasized that the small magnitude of the detected changes challenges the sensitivity of both microarray and qRT-PCR techniques. However, the rate of concordance between the two techniques was very reasonable, supporting the validity of the results.

In conclusion, the identification of a gene expression profile associated with reduced frataxin levels in this animal model provides valuable insights for further studies aimed at both understanding the earliest molecular events in FRDA pathogenesis, and in setting up in vitro tools to evaluate new therapeutic strategies.

Acknowledgments

We thank Coriell Cell Repositories for providing FRDA and control fibroblast cell lines, and Arnulf Koeppen, MD for critically reading the manuscript.

This work was supported by a research grant from Friedreich's Ataxia Research Alliance/MDA Seek-A-Miracle to GC and DHG, the William Smith Memorial fund gift to DHG, and by the National Institutes of Health (grant no. NS34192) to MP.

References

Acquaviva F, De Biase I, Nezi L, Ruggiero G, Tatangelo F, Pisano C, et al. Extra-mitochondrial localisation of frataxin and its association with IscU1 during enterocyte-like differentiation of the

human colon adenocarcinoma cell line Caco-2. J Cell Sci. 2005; 118:3917–3924. [PubMed: 16091420]

Andersen JK. Oxidative stress in neurodegeneration: cause or consequence? Nat Med. 2004; 10(Suppl):S18–S25. [PubMed: 15298006]

Arner ES, Holmgren A. Physiological functions of thioredoxin and thioredoxin reductase. Eur J Biochem. 2000; 267:6102–6109. [PubMed: 11012661]

Ben Hamida C, Doerflinger N, Belal S, Linder C, Reutenauer L, Dib C, et al. Localization of Friedreich ataxia phenotype with selective vitamin E deficiency to chromosome 8q by homozygosity mapping. Nat Genet. 1993; 5:195–200. [PubMed: 8252047]

Bidichandani SI, Ashizawa T, Patel PI. The GAA triplet-repeat expansion in Friedreich ataxia interferes with transcription and may be associated with an unusual DNA structure. Am J Hum Genet. 1998; 62:111–121. [PubMed: 9443873]

Boukhtouche F, Mariani J, Tedgui A. The "CholesteROR" protective pathway in the vascular system. Arterioscler Thromb Vasc Biol. 2004; 24:637–643. [PubMed: 14751813]

Campuzano V, Montermini L, Molto MD, Pianese L, Cossee M, Cavalcanti F, et al. Friedreich's ataxia: autosomal recessive disease caused by an intronic GAA triplet repeat expansion. Science. 1996; 271:1423–1427. [PubMed: 8596916]

Campuzano V, Montermini L, Lutz Y, Cova L, Hindelang C, Jiralerspong S, et al. Frataxin is reduced in Friedreich ataxia patients and is associated with mitochondrial membranes. Hum Mol Genet. 1997; 6:1771–1780. [PubMed: 9302253]

Cavadini P, O'Neill HA, Benada O, Isaya G. Assembly and iron-binding properties of human frataxin, the protein deficient in Friedreich ataxia. Hum Mol Genet. 2002; 11:217–227. [PubMed: 11823441]

Chang L, Karin M. Mammalian MAP kinase signalling cascades. Nature. 2001; 410:37–40. [PubMed: 11242034]

Chantrel-Groussard K, Geromel V, Puccio H, Koenig M, Munnich A, Rotig A, et al. Disabled early recruitment of antioxidant defenses in Friedreich's ataxia. Hum Mol Genet. 2001; 10:2061–2067. [PubMed: 11590123]

Cossee M, Puccio H, Gansmuller A, Koutnikova H, Dierich A, LeMeur M, et al. Inactivation of the Friedreich ataxia mouse gene leads to early embryonic lethality without iron accumulation. Hum Mol Genet. 2000; 9:1219–1226. [PubMed: 10767347]

Foury F, Talibi D. Mitochondrial control of iron homeostasis. A genome wide analysis of gene expression in a yeast frataxin-deficient strain. J Biol Chem. 2001; 276:7762–7768. [PubMed: 11112771]

Gerber J, Muhlenhoff U, Lill R. An interaction between frataxin and Isu1/Nfs1 that is crucial for Fe/S cluster synthesis on Isu1. EMBO Rep. 2003; 4:906–911. [PubMed: 12947415]

Geschwind DH. Mice, microarrays, and the genetic diversity of the brain. Proc Natl Acad Sci U S A. 2000; 97:10676–10678. [PubMed: 11005850]

Gohil K, Schock BC, Chakraborty AA, Terasawa Y, Raber J, Farese RV Jr, et al. Gene expression profile of oxidant stress and neurodegeneration in transgenic mice deficient in alpha-tocopherol transfer protein. Free Radical Biol Med. 2003; 35:1343–1454. [PubMed: 14642382]

Hamilton BA, Frankel WN, Kerrebrock AW, Hawkins TL, FitzHugh W, Kusumi K, et al. Disruption of the nuclear hormone receptor RORalpha in staggerer mice. Nature. 1996; 379:736–739. [PubMed: 8602221]

Helveston W, Hurd R, Uthman B, Wilder BJ. Abnormalities of glutathione peroxidase and glutathione reductase in four patients with Friedreich's disease. Mov Disord. 1996; 11:106–107. [PubMed: 8771081]

Hosack DA, Dennis G Jr, Sherman BT, Lane HC, Lempicki RA. Identifying biological themes within lists of genes with EASE. Genome Biol. 2003; 4:R70. [PubMed: 14519205]

Jiralerspong S, Ge B, Hudson TJ, Pandolfo M. Manganese superoxide dismutase induction by iron is impaired in Friedreich ataxia cells. FEBS Lett. 2001; 509:101–105. [PubMed: 11734214]

Karsten SL, Geschwind DH. Gene expression analysis using cDNA microarrays. Curr Prot Neurosci. 2002:4.28.1–4.28.28.

Karsten SL, Van Deerlin VM, Sabatti C, Gill LH, Geschwind DH. An evaluation of tyramide signal amplification and archived fixed and frozen tissue in microarray gene expression analysis. Nucleic Acids Res. 2002; 30:E4. [PubMed: 11788730]

Lamarche JB, Lemieux B, Lieu HB. The neuropathology of “typical” Friedreich’s ataxia in Quebec. Can J Neurol Sci. 1984; 11:592–600. [PubMed: 6509409]

Liang M, Briggs AG, Rute E, Greene AS, Cowley AW Jr. Quantitative assessment of the importance of dye switching and biological replication in cDNA microarray studies. Physiol Genomics. 2003; 14:199–207. [PubMed: 12799473]

Lutz T, Westermann B, Neupert W, Herrmann JM. The mitochondrial proteins Ssq1 and Jac1 are required for the assembly of iron sulfur clusters in mitochondria. J Mol Biol. 2001; 307:815–825. [PubMed: 11273703]

Miranda CJ, Santos MM, Ohshima K, Smith J, Li L, Bunting M, et al. Frataxin knockin mouse. FEBS Lett. 2002; 512:291–297. [PubMed: 11852098]

Muhlenhoff U, Richhardt N, Ristow M, Kispal G, Lill R. The yeast frataxin homolog Yfh1p plays a specific role in the maturation of cellular Fe/S proteins. Hum Mol Genet. 2002; 11:2025–2036. [PubMed: 12165564]

Pfaffl MW, Horgan GW, Dempfle L. Relative expression software tool (REST) for group-wise comparison and statistical analysis of relative expression results in real-time PCR. Nucleic Acids Res. 2002; 30:e36. [PubMed: 11972351]

Pianese L, Busino L, De Biase I, De Cristofaro T, Lo Casale MS, Giuliano P, et al. Up-regulation of c-Jun N-terminal kinase pathway in Friedreich’s ataxia cells. Hum Mol Genet. 2002; 11:2989–2996. [PubMed: 12393810]

Pianese L, Turano M, Lo Casale MS, De Biase I, Giacchetti M, Monticelli A, et al. Real time PCR quantification of frataxin mRNA in the peripheral blood leucocytes of Friedreich ataxia patients and carriers. J Neurol Neurosurg Psychiatry. 2004; 75:1061–1063. [PubMed: 15201375]

Puccio H, Koenig M. Friedreich ataxia: a paradigm for mitochondrial diseases. Curr Opin Genet Dev. 2002; 12:272–277. [PubMed: 12076669]

Puccio H, Simon D, Cossee M, Criqui-Filipe P, Tiziano F, Melki J, et al. Mouse models for Friedreich ataxia exhibit cardiomyopathy, sensory nerve defect and Fe–S enzyme deficiency followed by intramitochondrial iron deposits. Nat Genet. 2001; 27:181–186. [PubMed: 11175786]

Ristow M, Mulder H, Pomplun D, Schulz TJ, Muller-Schmehl K, Krause A, et al. Frataxin deficiency in pancreatic islets causes diabetes due to loss of beta cell mass. J Clin Invest. 2003; 112:527–534. [PubMed: 12925693]

Roy S, Lado BH, Khanna S, Sen CK. Vitamin E sensitive genes in the developing rat fetal brain: a high-density oligonucleotide microarray analysis. FEBS Lett. 2002; 530:17–23. [PubMed: 12387859]

Santos MM, Miranda CJ, Levy JE, Montross LK, Cossee M, Sequeiros J, et al. Iron metabolism in mice with partial frataxin deficiency. Cerebellum. 2003; 2:146–153. [PubMed: 12880182]

Schoenfeld RA, Napoli E, Wong A, Zhan S, Morin D, Buckpitt AR, et al. Frataxin deficiency alters heme pathway transcripts and decreases mitochondrial heme metabolites in mammalian cells. Hum Mol Genet. 2005; 14:3787–3799. [PubMed: 16239244]

Serra HG, Byam CE, Lande JD, Tousey SK, Zoghbi HY, Orr HT. Gene profiling links SCA1 pathophysiology to glutamate signaling in Purkinje cells of transgenic mice. Hum Mol Genet. 2004; 13:2535–2543. [PubMed: 15317756]

Seznec H, Simon D, Bouton C, Reutenauer L, Hertzog A, Golik P, et al. Friedreich ataxia, the oxidative stress paradox. Hum Mol Genet. 2005; 14:463–474. [PubMed: 15615771]

Shoichet SA, Baumer AT, Stamenkovic D, Sauer H, Pfeiffer AF, Kahn CR, et al. Frataxin promotes antioxidant defense in a thiol-dependent manner resulting in diminished malignant transformation in vitro. Hum Mol Genet. 2002; 11:815–821. [PubMed: 11929854]

Simon D, Seznec H, Gansmuller A, Carelle N, Weber P, Metzger D, et al. Friedreich ataxia mouse models with progressive cerebellar and sensory ataxia reveal autophagic neurodegeneration in dorsal root ganglia. J Neurosci. 2004; 24:1987–1995. [PubMed: 14985441]

Sipione S, Rigamonti D, Valenza M, Zuccato C, Conti L, Pritchard J, et al. Early transcriptional profiles in huntingtin-inducible striatal cells by microarray analyses. Hum Mol Genet. 2002; 11:1953–1965. [PubMed: 12165557]

Stehling O, Elsasser HP, Bruckel B, Muhlenhoff U, Lill R. Iron–sulfur protein maturation in human cells: evidence for a function of frataxin. Hum Mol Genet. 2004; 13:3007–3015. [PubMed: 15509595]

Sturm B, Bistrich U, Schranzhofer M, Sarsero JP, Rauen U, Scheiber-Mojdehkar B, et al. Friedreich's ataxia: no changes in mitochondrial labile iron in human lymphoblasts and fibroblasts: a decrease in antioxidative capacity? J Biol Chem. 2005; 280:6701–6708. [PubMed: 15615730]

Tan G, Napoli E, Taroni F, Cortopassi G. Decreased expression of genes involved in sulfur amino acid metabolism in frataxin-deficient cells. Hum Mol Genet. 2003; 12:1699–1711. [PubMed: 12837693]

Watts JA, Morley M, Burdick JT, Fiori JL, Ewens WJ, Spielman RS, et al. Gene expression phenotype in heterozygous carriers of ataxia telangiectasia. Am J Hum Genet. 2002; 71:791–800. [PubMed: 12226795]

Yang YH, Dudoit S, Luu P, Lin DM, Peng V, Ngai J, et al. Normalization for cDNA microarray data: a robust composite method addressing single and multiple slide systematic variation. Nucleic Acids Res. 2002; 30:e15. [PubMed: 11842121]

Yokota T, Igarashi K, Uchihara T, Jishage K, Tomita H, Inaba A, et al. Delayed-onset ataxia in mice lacking alpha -tocopherol transfer protein: model for neuronal degeneration caused by chronic oxidative stress. Proc Natl Acad Sci U S A. 2001; 98:15185–15190. [PubMed: 11752462]

Yoshihara T, Ishigaki S, Yamamoto M, Liang Y, Niwa J, Takeuchi H, et al. Differential expression of inflammation- and apoptosis-related genes in spinal cords of a mutant SOD1 transgenic mouse model of familial amyotrophic lateral sclerosis. J Neurochem. 2002; 80:158–167. [PubMed: 11796754]

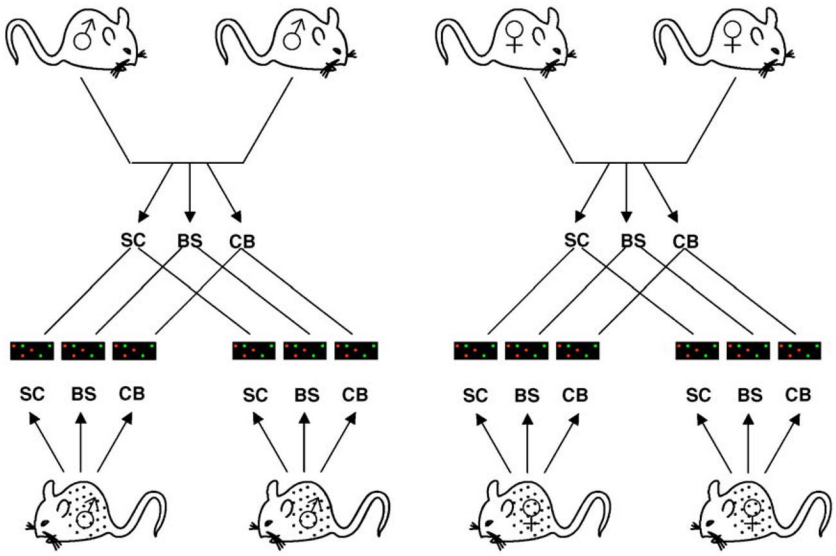

Fig. 1.

Study design schematic. Four 6-month-old KIKO mice (2 males, 2 females) were compared to age and gender matched WT littermates. RNA extracted from each of three CNS regions was co-hybridized on microarray slides (n = 12, 4 for spinal cord, 4 brainstem, and 4 cerebellum). To control for biological variability, WT samples from the same gender were pooled. To avoid a dye-effect, replicates were performed with dye-swaps, for a total of 24 array hybridizations performed (8 for spinal cord, 8 brainstem, and 8 cerebellum). SC: spinal cord; BS: brainstem; CB: cerebellum.

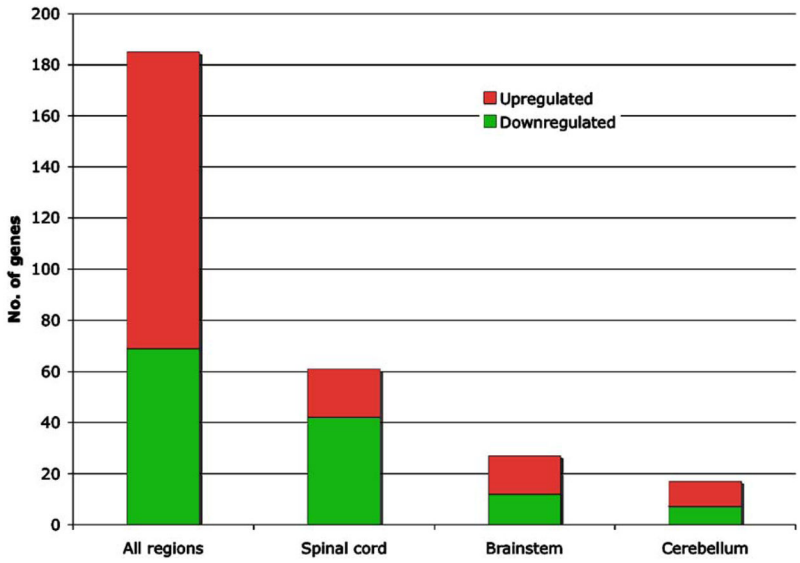

Fig. 2.

Differentially expressed genes in three CNS regions in frataxin deficient mice. 185 genes were identified as differentially expressed across all regions. An additional 105 genes showed expression changes with a regional distribution, following the gradient of known neuropathological involvement in FRDA (spinal cord > brainstem > cerebellum). The majority of these changes were observed in the cervical spinal cord, the most severely affected region in patients, and most of them were towards downregulation.

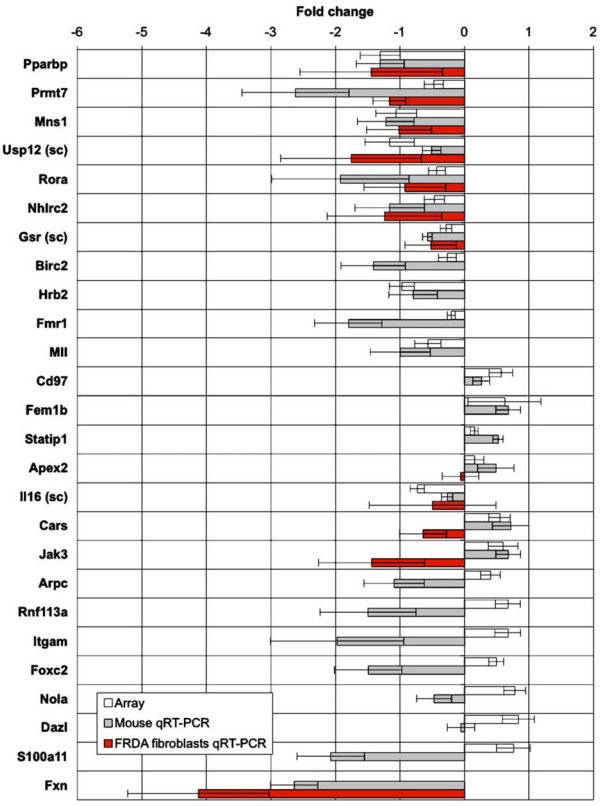

Fig. 3.

Microarray and qRT-PCR data in KIKO mice and FRDA fibroblasts. Microarray data were confirmed through real-time quantitative PCR. Samples from at least 3 distinct animals and controls were tested. A subset of genes was tested on three fibroblast cell lines from FRDA patients. Two genes with regional changes in spinal cord (sc) were also observed to be differentially expressed in human fibroblasts. Frataxin (bottom row) was not present on the array, so we present qRT-PCR data showing its downregulation in both KIKO mice and FRDA fibroblasts. Bars: fold change. Error bars: standard error.

Table 1

Differentially expressed genes between KIKO and control mice

Accession no.	Symbol	Description	All	SC	CB	BS
Nucleobase, nucleoside, nucleotide and nucleic acid metabolism						
AA030303	**Fem1b**	**Feminization 1 homolog b (*C. elegans*)**[§]	+0.5			
W11649	**Cars**	**Cysteinyl-tRNA synthetase**[§]	+0.5			
AA176045	**Foxc2**	**Forkhead box C2**	+0.5			
AA404192	Imp4	IMP4, U3 small nucleolar ribonucleoprotein, homolog (yeast)	+0.4			
AA122544	Prpf3	PRP3 pre-mRNA processing factor 3 homolog (yeast)	+0.3			
AA423717	**Apex2**	**Apurinic/apyrimidinic endonuclease 2**[§]	+0.3			
AA170595	Sfrs1	Splicing factor, arginine/serine-rich 1 (ASF/SF2)	+0.3			
AA237894	Prim2	DNA primase, p58 subunit	+0.3			
AA265966	Strap	Serine/threonine kinase receptor associated protein	+0.3			
W66622	Tead2	TEA domain family member 2	+0.3			
AA177814	Smad1	MAD homolog 1 (*Drosophila*)	+0.2			
AA152649	**Pparbp**	**Peroxisome proliferator activated receptor binding protein**[§,¶]	−1.2			
AA060386	**Mll**	**Myeloid/lymphoid or mixed-lineage leukemia**[§]	−0.5			
AA028383	2700067D09Rik	RIKEN cDNA 2700067D09 gene	−0.5			
AA038717	**Rora**	**RAR-related orphan receptor alpha**[§,¶]	−0.4			
AA139711	Rnf134	Ring finger protein 134		**+1.3**	−0.4	−0.1
AA250500	Pttg1	Pituitary tumor-transforming 1		**+0.3**	0.0	0.0
W98988	Orc3l	Origin recognition complex, subunit 3-like (*S. cerevisiae*)		**−0.4**	+0.1	+0.3
AA189879	Zfp277	Zinc finger protein 277		**−0.3**	+0.1	+0.1
AA050578	Asb10	Ankyrin repeat and SOCS box-containing protein 10		−0.4	**+0.6**	−0.3
AA242567	Sra1	Steroid receptor RNA activator 1		−0.3	−0.3	**0.8**
AA146020	Zfp275	Zinc finger protein 275		0.0	+0.1	**−0.4**
Protein metabolism						
AA467406	Mrpl34	Mitochondrial ribosomal protein L34	+0.3			
W16221	Col6a1	Procollagen, type VI, alpha 1	+0.3			
AA175583	Mrpl39	Mitochondrial ribosomal protein L39	+0.2			

Accession no.	Symbol	Description	All	SC	CB	BS
AA164013	Rps6	Ribosomal protein S6	−0.4			
CB035345	Padi2	Peptidyl arginine deiminase, type II	−0.3			
AA261590	Kel	Kell blood group	−0.3			
AA422887	Pum2	Pumilio 2 (*Drosophila*)	−0.2			
AA087036	Arl6ip1	ADP-ribosylation factor-like 6 interacting protein 1	−0.2			
AA051390	Pin1	Protein (peptidyl-prolyl cis/trans isomerase) NIMA-interacting 1		**0.3**	0.0	−0.2
AA013513	**Usp12**	**Ubiquitin-specific protease 12**[§,¶]		**−1.0**	0.5	0.1
Cell growth and/or maintenance						
AA177702	Slc25a30	Solute carrier family 25, member 30	0.3			
W13243	Apg16l	APG16 autophagy 16-like (*S. cerevisiae*)	0.2			
AA000328	Mad2l1bp	MAD2L1 binding protein	−0.8			
AA060483	Nolc1	Nucleolar and coiled-body phosphoprotein 1	−0.2			
AA000093	Kdelr1	KDEL endoplasmic reticulum protein retention receptor 1		**0.9**	−0.2	0.0
AA162446	Ryr1	Ryanodine receptor 1, skeletal muscle		**−0.7**	0.1	0.1
AA003205	Kif22	Kinesin family member 22		**−0.6**	0.3	0.3
W96925	Mscp	Mitochondrial solute carrier protein		**−0.6**	0.1	0.2
AA466838	Cdc5l	Cell division cycle 5-like (*S. pombe*)		**−0.3**	0.1	0.1
AA144080	Ski	Sloan-Kettering viral oncogene homolog		−0.4	−0.8	**1.0**
Signal transduction						
AA061908	**Itgam**	**Integrin alpha M**	0.6			
AA080529	**Cd97**	**CD97 antigen**[§]	0.5			
AA023670	**Jak3**	**Janus kinase 3**[§]	0.5			
AA267811	Lcp2	Lymphocyte cytosolic protein 2		**−0.7**	+0.2	+0.1
AA023159	Stat1	Signal transducer and activator of transcription 1		**−0.6**	+0.0	+0.0
AA163237	Epha3	Eph receptor A3		−0.6	**+1.6**	+0.0
AA050000	Rasa3	RAS p21 protein activator 3		−0.1	−0.1	**+0.4**
RNA binding						
AA049897	**Nola1**	**Nucleolar protein family A, member 1**	+0.7			
AA414507	**Dazl**	**Deleted in azoospermia-like**	+0.7			
AA138018	**Mrps28**	**Mitochondrial ribosomal protein S28**	+0.2			
AA200033	**Fmr1**	**Fragile X mental retardation syndrome 1 homolog**[§]	−0.3			

Accession no.	Symbol	Description	All	SC	CB	BS
RNA binding						
AA185249	2810028N01Rik	RIKEN cDNA 2810028N01 gene		+0.1	**+1.1**	−0.5
W08137	D19Bwg1357e	DNA segment, Chr 19, Brigham and Women's Genetics 1357 expressed		+0.1	**−0.3**	+0.2
DNA binding						
AA25451	**Rnf113a**	**Ring finger protein 113A**	+0.5			
AA386522	E430027O22Rik	RIKEN cDNA E430027O22 gene	+0.3			
AA146460	Zranb3	Zinc finger, RAN-binding domain containing 3	+0.4			
AA426942	Pole4	Polymerase (DNA-directed), epsilon 4 (p12 subunit)	+0.2			
AA049607	Terf2	Telomeric repeat binding factor 2	−0.3			
W62349	Centa1	Centaurin, alpha 1		**+0.2**	−0.2	0.0
Electron transport						
AA049211	Cyb5m	Cytochrome b5 outer mitochondrial membrane precursor	−0.4			
AA125257	**Nhlrc2**	**NHL repeat containing 2**[§,¶]	−0.4			
AA473629	Cyp2j5	Cytochrome P450, family 2, subfamily j, polypeptide 5		**−0.5**	+0.2	+0.2
AA177872	**Gsr**	**Glutathione reductase 1**[§,¶]		**−0.4**	+0.3	+0.1
Nucleic acid binding						
AA185944	**Hrb2**	**HIV-1 Rev binding protein 2**[§]	−0.8			
AA266342	Trim25	Tripartite motif protein 25	−0.4			
AA290538	Rdbp	RD RNA-binding protein	−0.3			
AA183836	Mbnl2	Muscleblind-like 2		0.0	**+0.2**	0.0
Cytokine activity						
AA178155	Ccl4	Chemokine (C–C motif) ligand 4		**−0.9**	+0.3	+0.5
AA155344	**Il16**	**Interleukin 16**[§]		**−0.7**	0.0	+0.4
W98440	Fgf23	Fibroblast growth factor 23		**−0.4**	+0.2	+0.1
Other						
AA253928	**S100a11**	**S100 Calcium binding protein A11 (calizzarin)**	+0.6			
AA060715	Scrn3	Secernin 3	+0.5			
AA064058	**Arpc2**	**Actin related protein 2/3 complex, subunit 2**	+0.5			
AA462270	Syngap1	Synaptic Ras GTPase activating protein 1 homolog (rat)	+0.4			
AA051422	Ak3l	Adenylate kinase 3 alpha-like	+0.4			
AA052194	Parc	P53-associated parkin-like cytoplasmic protein	+0.4			

Neurobiol Dis. Author manuscript; available in PMC 2010 June 15.

Accession no.	Symbol	Description	All	SC	CB	BS
AA260621	AI132487	Mitochondrial hepatocellular carcinoma-downregulated carrier protein	+0.4			
W65895	Snapc5	Small nuclear RNA activating complex, polypeptide 5	+0.4			
AA118848	Ncstn	Nicastrin	+0.3			
AA387002	Mrps30	Mitochondrial ribosomal protein S30	+0.3			
AA517261	Katnb1	Katanin p80 (WD40-containing) subunit B 1	+0.3			
AA183022	Map4k5	Mitogen-activated protein kinase kinase kinase kinase 5	+0.2			
AA057998	**Mns1**	**Meiosis-specific nuclear structural protein 1**[§,¶]	−0.9			
BF642807	Tmed5	Transmembrane emp24 protein transport domain containing 5	−0.7			
AA050341	Rps26	Ribosomal protein S26	−0.5			
AA208770	Itih2	Inter-alpha trypsin inhibitor, heavy chain 2	−0.5			
AA125257	**Prmt7**	**protein arginine N-methyltransferase 7**[§,¶]	−0.4			
AA197349	**Birc2**	**Baculoviral IAP repeat-containing 2**[§]	−0.4			
CA748288	Lypla1	Lysophospholipase 1	−0.3			
AA268671	Csnk1a1	Casein kinase 1, alpha 1	−0.3			
AA052356	Ppm1m	Protein phosphatase 1M	−0.2			
W85052	Galnt11	UDP-GalNAc:polypeptide N-acetylgalactosaminyltransferase		**+0.9**	−0.1	−0.2
AA002886	Ddx51	DEAD (Asp–Glu–Ala–Asp) box polypeptide 51		**+0.7**	−0.4	−0.4
W08172	Sgpl1	Sphingosine phosphate lyase 1		**+0.4**	−0.1	0.0
AA387369	Pmm1	Phosphomannomutase 1		**+0.3**	0.0	−0.1
W59202	**Statip1**	**STAT3 interacting protein 1**[§]		**+0.2**	+0.1	−0.1
AA154417	Mak3	Mak3p homolog (*S. cerevisiae*)		**−0.6**	+0.1	0.0
W08694	Car4	Carbonic anhydrase 4		**−0.5**	0.0	+0.4
AA288611	Ulk2	Unc-51 like kinase 2 (*C. elegans*)		**−0.4**	0.0	+0.1
Other						
AA474389	Ddc	Dopa decarboxylase		0.0	**+0.5**	−0.1
AA423601	Osbpl11	Oxysterol binding protein-like 11		+0.1	**+0.5**	0.0
AA286352	Nup107	Nucleoporin 107		+0.1	**−0.4**	+0.2
AA125271	Cyb561d1	Cytochrome b-561 domain containing 1		−0.4	−0.1	**+1.5**
AA217892	Habp2	Hyaluronic acid binding protein 2		+0.4	+0.3	**−0.3**
Unknown						
W29916	D19Wsu12e	DNA segment, Chr 19, Wayne State University 12, expressed	+0.6			

Accession no.	Symbol	Description	All	SC	CB	BS
W66885	BC019943	cDNA sequence BC019943	+0.4			
AA474452	Mbtd1	mbt domain containing 1	+0.3			
AA152739	4930438O05Rik	RIKEN cDNA 4930438O05 gene	+0.3			
AA422515	D5Ertd135e	DNA segment, Chr 5, ERATO Doi 135, expressed	+0.3			
AA265198	1200003E16Rik	RIKEN cDNA 1200003E16 gene	+0.3			
AA168435	AI447928	Expressed sequence AI447928	+0.3			
AA145822	D330037H05Rik	RIKEN cDNA D330037H05 gene	+0.3			
AA212455	4932414K18Rik	RIKEN cDNA 4932414K18 gene	+0.2			
AA178792	Takrp	T-cell activation kelch repeat protein	+0.2			
AA435335	2610029D06Rik	Zinc finger CCCH type domain containing 3	+0.2			
AA002332	AB023957	cDNA sequence AB023957	−0.7			
AA060599	4921525L17Rik	RIKEN cDNA 4921525L17 gene	−0.7			
W99838	Dab2ip	Disabled homolog 2 (*Drosophila*) interacting protein	−0.4			
CA748358	AA792894	EST AA792894	−0.3			
AA027647	AW121567	expressed sequence AW121567	−0.3			
AA110273	Gm711	Gene model 711, (NCBI)	−0.2			
AA060255	Ylpm1	YLP motif containing 1	−0.2			
AA031108	1200003M09Rik	RIKEN cDNA 1200003M09 gene		**+0.5**	−0.1	−0.2
W58977	A330068P14Rik	RIKEN cDNA A330068P14 gene		**+0.3**	−0.1	−0.1
W89976	Mdm1	Transformed mouse 3T3 cell double minute 1		**−0.4**	+0.1	+0.1
AA432477	Spire1	Spire homolog 1 (*Drosophila*)		**−0.4**	+0.3	+0.3
AA203889	Gm525	gene model 525, (NCBI)		+0.2	**−0.9**	+0.2
AA028632	Gm131	similar to prochymosin		−0.1	+0.1	**+2.8**
AA218073	2810474O19Rik	RIKEN cDNA 2810474O19 gene		−0.3	−0.3	**+0.7**
W16162	2900073H19Rik	RIKEN cDNA 2900073H19 gene		−0.5	−0.3	**+0.5**
AA290313	1810009A15Rik	RIKEN cDNA 1810009A15 gene		−0.7	−0.1	**+0.5**
AA109106	1200002M06Rik	RIKEN cDNA 1200002M06 gene		+0.1	+0.1	**−1.6**
W59073	1300001I01Rik	RIKEN cDNA 1300001I01 gene		0.0	0.0	**−0.3**

Differential expression is expressed as fold change. Fold changes in bold: $P < 0.01$ (ANOVA). SC: spinal cord; CB: cerebellum; BS: brainstem. Genes in bold have been tested with RT-PCR:

§ confirmed in KIKO mice;

¶ confirmed in FRDA fibroblasts.

Table 2

Gene ontology categorization and EASE analysis

Gene category	List hits	List total	Population hits	Population total	EASE score
GO biological process					
Ribosome biogenesis	5	151	29	3804	0.03
GO cellular component					
Mitochondrion	19	159	271	3795	0.03
Ribonucleoprotein complex	14	159	146	3795	0.01
Spliceosome complex	5	159	33	3795	0.05
GO molecular function					
Nucleic acid binding	53	167	879	3986	0.00
RNA binding	15	167	168	3986	0.01